"Cut-and-Paste" Manufacture of Multiparametric Epidermal Sensor Systems

*Shixuan Yang, Ying-Chen Chen, Luke Nicolini, Praveenkumar Pasupathy, Jacob Sacks, Becky Su, Russell Yang, Daniel Sanchez, Yao-Feng Chang, Pulin Wang, David Schnyer, Dean Neikirk, and Nanshu Lu**

Our body is radiating data about ourselves continuously and individually. Wearable devices that can pick up and transmit signals from the human body have the potential to transform mobile health (mHealth) and human–machine interface (HMI), which prompted the Forbes Magazine to name 2014 as the year of wearable technology.[1] However, since wafer-based integrated circuits are planar, rigid, and brittle, state-of-the-art wearable devices are mostly in the form factors of "chips on tapes" or "bricks on straps," which are unable to maintain intimate and prolonged contact with the curved, soft, and dynamic human body for long-term, high-fidelity physiological signal monitoring.[2]

Recent advancements in flexible and stretchable electronics have provided viable solutions to bio-mimetic electronic skins[3–5] and bio-integrated electronics.[6,7] Among many breakthroughs, epidermal electronic systems (EES) represent a paradigm-shift wearable device whose thickness and mechanical properties can match that of human epidermis.[8] As a result, the EES can conform to human skin like a temporary transfer tattoo and deform with the skin without detachment or fracture. The EES was first developed to monitor electrophysiological (EP) signals,[8] and thereafter skin temperature,[9,10] skin hydration,[11–13] sweat,[14,15] and even movement disorders.[16] Moreover, near field communication (NFC) antenna based on EES technology has also been reported.[13,15,17]

The thinness and softness of EES, however, lead to collapsing and crumpling after it is peeled off human skin, making its use as a disposable electronic tattoo ideal. As a result, the success of EES hinges on the realization of low-cost, high-throughput manufacture. Current EES manufacture relies on standard microelectronics fabrication processes including vacuum deposition of films, spin coating, photolithography, wet and dry etching, as well as transfer-printing.[8,13,17] Although it has been proved effective, there are several limitations associated with such process: first, a rigid handle wafer has to be used for photolithography, making it incompatible with roll-to-roll process; second, the high cost associated with cleanroom facilities, photo masks, photolithography chemicals, and manpower prevents EES from being inexpensive and disposable; third, high vacuum film deposition is time consuming and hence impractical for growing thick films; fourth, the EES size is confined by the size of the handle wafer, whose size is limited by the smallest vacuum chamber throughout the process; and last but not least, the high manpower demand of the manufacturing process greatly limits the accessibility of EES.

Our newly invented "cut-and-paste" method offers a very simple and immediate solution to the above mentioned challenges. Instead of high vacuum metal deposition, thin metal-on-polymer laminates of various thicknesses can be directly purchased from industrial manufacturers. Instead of using photolithography patterning, a benchtop programmable cutting machine is used to mechanically carve out the patterns as designed, with excess being removed, which is a freeform, subtractive manufacturing process, inverse to the popular freeform, additive manufacturing technology.[18] The cutting machine can pattern on thin sheet metals and polymers up to 12 inches wide and several feet long, largely exceeding lab-scale wafer sizes. Since the patterns can be carved with the support of thermal release tapes (TRTs), whose adhesive can be released after heating, the patterned films can be directly printed onto a variety of tattoo adhesives and medical tapes with almost 100% yield. The whole process can be completed on an ordinary bench within 10 min without any wet process, which allows rapid prototyping. Equipment used in this process only includes a desktop cutting machine for thin film patterning and a hot plate for TRT heating, which enables portable manufacture. Since no rigid handle wafer is needed throughout the process, the "cut-and-paste" method is intrinsically compatible with roll-to-roll manufacture. To demonstrate the "cut-and-paste" method, multimaterial epidermal sensor systems

S. Yang, Y.-C. Chen, L. Nicolini, J. Sacks, B. Su, R. Yang, D. Sanchez, Dr. Y.-F. Chang, Dr. P. Wang, Prof. N. Lu
Center for Mechanics of Solids, Structures and Materials
Department of Aerospace Engineering and Engineering Mechanics
University of Texas at Austin
Austin, TX 78712, USA
E-mail: nanshulu@mail.utexas.edu

Y.-C. Chen, P. Pasupathy, Dr. Y.-F. Chang, Prof. D. Neikirk
Department of Electrical and Computer Engineering
University of Texas at Austin
Austin, TX 78712, USA

L. Nicolini, Prof. N. Lu
Texas Materials Institute
University of Texas at Austin
Austin, TX 78712, USA

Prof. D. Schnyer
Department of Psychology
University of Texas at Austin
Austin, TX 78712, USA

Prof. N. Lu
Department of Biomedical Engineering
University of Texas at Austin
Austin, TX 78712, USA

DOI: 10.1002/adma.201502386

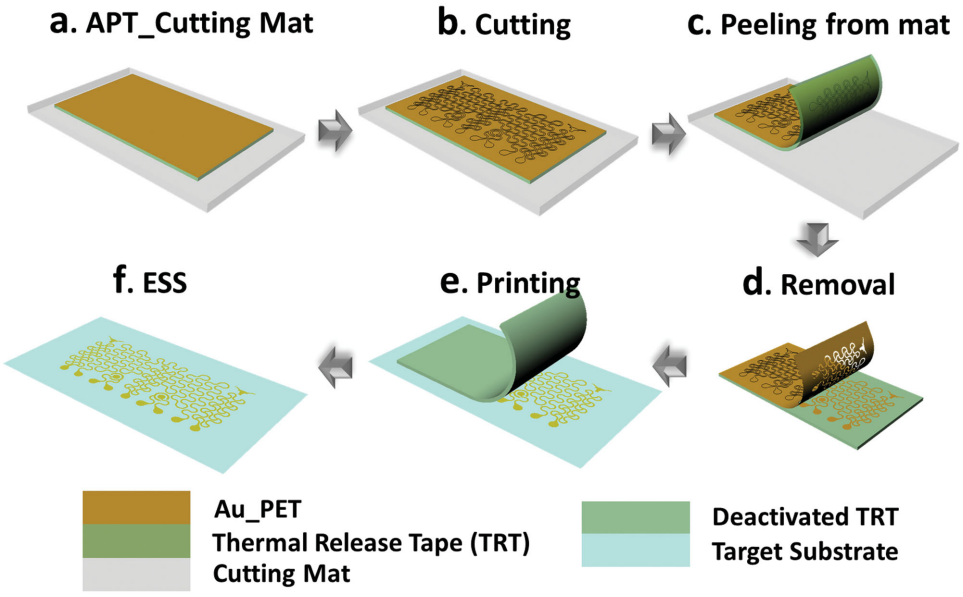

Figure 1. Schematics for the "cut-and-paste" process. a) Au-PET-TRT (APT) laminated on the cutting mat with PET being the topmost layer. b) Carving designed seams in the Au-PET layer by an automated mechanical cutting machine. c) Peeling APT off the cutting mat. d) Removing excessive Au-PET layer after deactivating the TRT on hot plate. e) Printing patterned Au-PET layer onto target substrate. f) Resulted epidermal sensor system (ESS) with Au being the topmost layer.

(ESS) are fabricated and applied to measure EP signals such as electrocardiogram (ECG), electromyogram (EMG), electroencephalogram (EEG), skin temperature, skin hydration, and respiratory rate. A planar stretchable coil of 9-μm-thick aluminum ribbons exploiting the double-stranded serpentine design is also integrated on the ESS as a MHz frequency, wireless strain gauge, which can also serve as NFC antenna in the future.

A schematic of the freeform "cut-and-paste" process is shown in **Figure 1**. Since stiff-polymer-supported blanket metal films are more stretchable than freestanding metal sheets,[19] we always use metal-on-stiff-polymer laminates as the starting materials. Starting materials such as gold (Au) coated polyimide and aluminum (Al) coated polyethylene terephthalate (PET) are commonly used as thermal control or cable shielding laminates and can be purchased from industrial suppliers such as Sheldahl (Northfield, MN) and Neptco (Pawtucket, RI). We were able to purchase a small roll of 9-μm-thick Al on 12-μm-thick PET laminates from Neptco. Since only a small amount of polymer-supported Au foils are used in this research but industrial quantity can be very expensive, we chose to use thermal evaporation to deposit several batches of 100-nm-thick Au films on 13-μm-thick transparent PET foils (Goodfellow, USA). A picture of the Au-on-PET foil is shown in Supporting Information Figure S1a. To manufacture Au-based stretchable EP electrodes, resistance temperature detectors (RTDs), and impedance sensors, the Au-on-PET foil was uniformly bonded to a flexible, single-sided TRT (Semiconductor Equipment Corp., USA) with Au side touching the adhesive of the TRT, as shown in Supporting Information Figure S1b. The other side of the TRT was then adhered to a tacky flexible cutting mat, as shown in Figure 1a and Supporting Information Figure S1c. The cutting mat was fed into a programmable cutting machine (Silhouette Cameo, USA) with the PET side facing the cutting blade. By importing our AutoCAD design into the Silhouette Studio software, the cutting machine can automatically carve the Au-on-PET sheet with designed seams within minutes (Figure 1b and Supporting Information Figure S1d). Once seams were formed, the TRT was gently peeled off from the cutting mat (Figure 1c and Supporting Information Figure S1e). Slightly baking the TRT on a 115 °C hotplate for 1–2 min (Supporting Information Figure S1f) deactivated the adhesives on the TRT so that the excesses can be easily peeled off by tweezers (Figure 1d and Supporting Information Figure S1g), leaving only the EP electrodes, RTD, and impedance sensors loosely resting on the TRT. The patterned devices were finally printed onto a target substrate with native adhesives, which could be a temporary tattoo paper (Silhouette) or a medical tape, such as 3M Tegaderm transparent dressing or 3M kind removal silicone tape (KRST) (Figure 1e and Supporting Information Figure S1h), yielding a Au-based ESS (Figure 1f and Supporting Information Figure S1i). Steps illustrated by Figure 1a–e can be repeated for other thin sheets of metals and polymers, which can be printed on the same target substrate with alignment markers, rendering a multimaterial, multiparametric ESS ready for skin mounting.

A multimaterial, multiparametric ESS supported by transparent temporary tattoo paper and its white liner is shown in **Figure 2**a, which includes three Au-based filamentary serpentine (FS) EP electrodes, one Au-based FS RTD, two Au-based dot-ring impedance sensors, and an Al-based planar stretchable coil. In this picture, all Au-based sensors have the Au side facing up and in the future touching human skin as Au is a biocompatible metal. The stretchable coil, however, has the blue colored PET facing up because PET has demonstrated good biocompatibility[20] but some people's skin can be allergic to Al. For the three EP electrodes, the interelectrode distance is

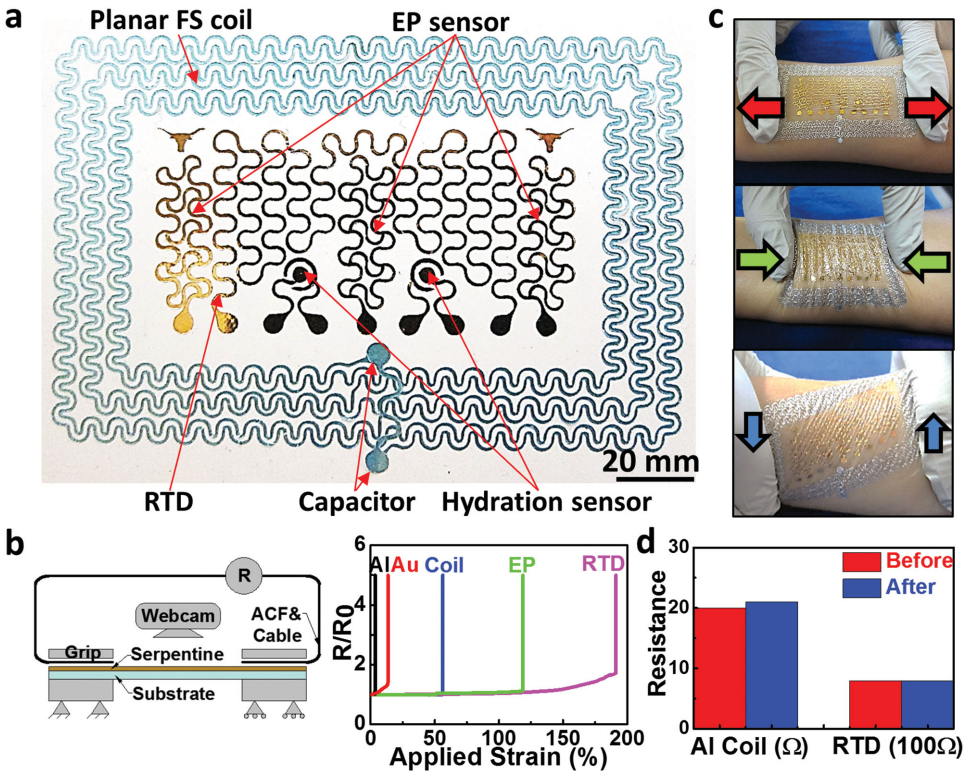

Figure 2. Multimaterial, multiparametric ESS. a) Top view of an ESS which incorporates three electrophysiological (EP) electrodes (Au-PET), a resistance temperature detector (RTD) (Au-PET), two coaxial dot-ring impedance sensors (Au-PET), and a wireless planar stretchable strain sensing coil (Al-PET), all in filamentary serpentine (FS) layout. b) Resistance change measured as function of applied strain. "Al" denotes straight Al-PET ribbon, "Au" denotes straight Au-PET ribbon, "Coil" denotes Al-PET serpentine ribbon used in wireless strain sensor coil, "EP" denotes Au-PET serpentine ribbon used in EP electrode, and "RTD" denotes Au-PET serpentine ribbon used in RTD. c) ESS on human skin demonstrating excellent deformability during stretch (top), compression (middle), and shear (bottom). d) Resistance of Al coil and Au RTD before and after all possible deformations of skin-mounted ESS.

set to be 2 cm for effective EP signal recording.[21] The FS is designed with a 1/5 ribbon width to arc radius ratio in order to balance the trade-off between stretchability and occupied area, according to our recent mechanics of serpentine research.[22] The same FS design is not applicable to the stretchable Al coil because it will consume too much space when many turns are needed for higher inductance. Therefore a double-stranded serpentine design is proposed (Figure 2a), which saves space without compromising the number of turns or the stretchability too much. The two longhorns at the upper left and right corners of the Au pattern serve as alignment markers for printing Au and Al devices on the same tape. The overall size of the device area is 7.5 cm × 5 cm. Detailed quality examination of "cut-and-paste" manufactured specimens is provided in Supporting Information Figures S2–S4.

The Young's moduli of the different materials used in ESS and ESS itself are measured by uniaxial tension tests using an RSA-G2 dynamic mechanical analyzer (TA Instruments) and summarized in Supporting Information Figure S5 and Supporting Information Table S1. Out of all substrate materials that have been tested, including tattoo paper, Tegaderm, and KRST, Tegaderm is the most compliant one. It's modulus (7.4 MPa) is close to the high end of the modulus of human skin (0.32–4 MPa[23]) Supporting Information Figure S5c shows that Tegaderm is composed of a backing layer and an adhesive layer. Using a scotch tape to peel the adhesive layer off the backing layer, we measured the stress–strain curves of each layer as shown in Supporting Information Figure S5d.

The stretchability of different serpentine ribbons on Tegaderm tapes was tested using a customized tensile tester with in situ resistance measurement and top down webcam observation (Figure 2b, left panel).[24] When electrical resistance is measured as a function of the applied uniaxial tensile strain, the applied strain at which the resistance explodes (e.g., $R/R_0 = 1.1$) is considered the strain-to-rupture or stretchability.[19] According to Figure 2b, right panel, while straight Al-on-PET and Au-on-PET ribbons exhibit limited stretchability (2.89% and 13.72%, respectively), their serpentine-shaped ribbons as shown in Supporting Information Figure S6a (Al coil), S6b (Au EP electrode), and S6c (Au RTD) are much more stretchable, well beyond the elastic limit of human skin (30%).[25] For serpentine ribbons such as the Al coil and Au RTD, rupture sites are always found at the crest of the arc (Supporting Information Figure S6a,c), whereas for serpentine network such as the Au EP electrode, fracture occurs first at ribbon intersections (Supporting Information Figure S6b) due to strain concentration and overcutting at turning points (Supporting Information Figure S4d–i). Cycleability of the Au serpentine was tested on an RSA-G2 dynamic mechanical analyzer (TA Instruments) with a frequency of 2 Hz. Supporting Information Figure S7 displays the resistance change of the Au serpentine as a function of the number of cycles. When applied strain is 20%, the

Au serpentine can be stretched 10 000 times before the resistance increases by 1%.

Supporting Information Figure S8 displays ESS on three different types of substrates and how they can be applied to human skin. While Tegaderm and tattoo papers are thin, transparent, and truly skin-like (Supporting Information Figure S8a–h), the KRST is much thicker and behaves like a cloth tape (Supporting Information Figure S8i–l). Because of the thickness, KRST does not crumple after being peeled off from the skin and the silicone adhesive allows multiple attachment and detachment before losing adhesion. Skin–ESS interaction is shown in Figure 2c and more in Supporting Information Figure S9, which validates the tattoo-like mechanics of the ESS. The electrical resistance of the Al and Au serpentines before and after various kinds of skin deformation (stretching, compression, shear, poking, etc.) is provided in Figure 2d. It is evident that the ESS can survive all possible skin deformations without any mechanical degradation.

The multiparametric ESS has been successfully applied to perform continuous EP, skin temperature, and skin hydration measurements. EP signals on the surface of human skin measure the flow of ions in the underneath tissues and organs, which reflects their health and function. For example, noninvasive ambulatory monitoring of ECG on human chest can help detect multiple important features of heart malfunction like irregular heartbeat (arrhythmia).[26] EMG reflects human muscle activity and can identify neuromuscular diseases and serve as a control signal for prosthetic devices or other machines.[21] EEG measured from the surface of human scalp can be used to not only capture cognitive and memory performance[27] but also chart brain disorders like epilepsy[28] and stroke.[29] **Figure 3**a displays ECG measurement from human chest using silver/silver chloride (Ag/AgCl) gel electrodes and the ESS without applying any conductive gels. Both ESS and Ag/AgCl electrodes were connected to a small portable amplifier (AvatarEEG) with a shared ground port through a homemade reusable connector (Supporting Information Figure S10). Out of the three EP electrodes integrated on the ESS, the center one is utilized as a ground and the other two electrodes measure EP signals in a bipolar montage to reflect the difference in electrical potential. Signals recorded by AvatarEEG were processed using a Principle Component Analysis based algorithm,[30] with the final results shown in Figure 3a. It is evident that the important features of ECG are captured by both electrodes, but the ECG measured by our ESS demonstrates higher amplitude. We also placed the same type of ESS over the forearm, specifically on the flexor muscles, to measure the EMG during two hand clenches (Figure 3b). The intensity of the gripping force can be measured by a commercial dynamometer (Exacta) and it is clear that the higher gripping force corresponds to higher signal amplitude in the EMG. Finally, we measured EEG by adhering Ag/AgCl electrodes and the ESS on human forehead. Both electrodes were referenced against one FS electrode placed behind the human

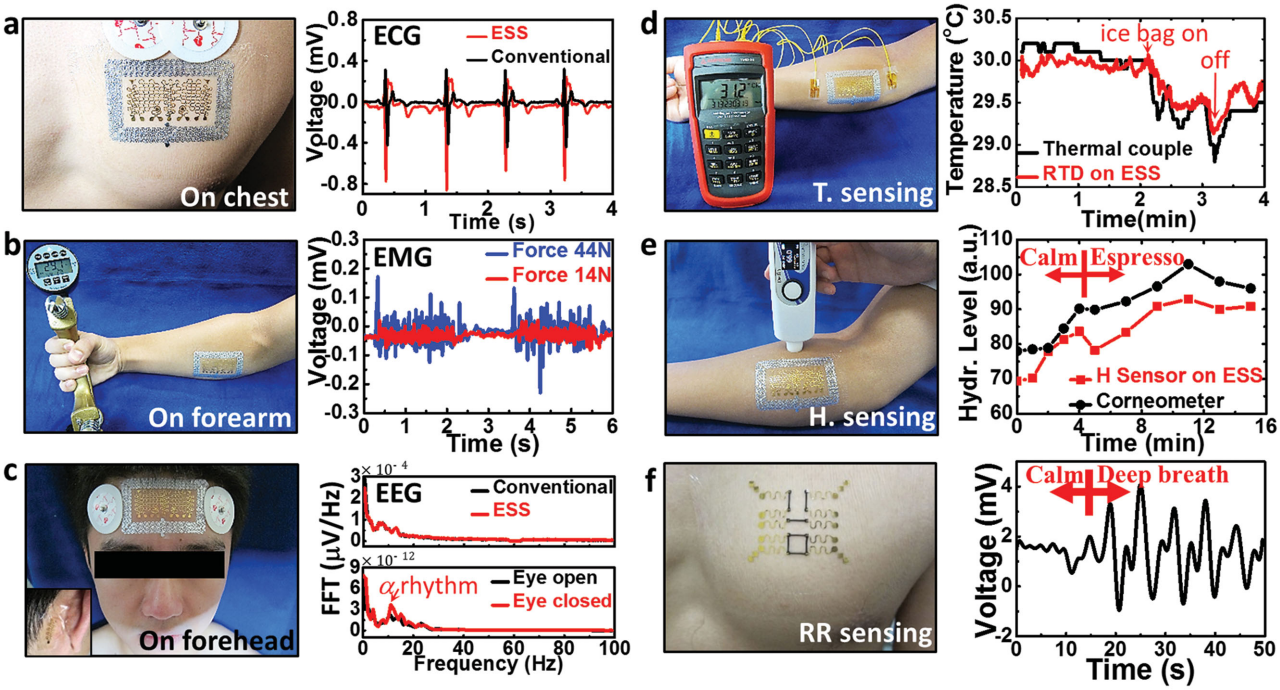

Figure 3. ECG, EMG, EEG, skin temperature, skin hydration, and respiratory rate measurements by ESS. a) ECG simultaneously measured by ESS (red) and Ag/AgCl electrodes (black). Stronger ECG signals were obtained by the ESS. b) ESS attached on human forearm for EMG measurement when the subject is gripping a commercial dynamometer with different forces. EMG of higher amplitude (blue) corresponds to higher gripping force. c) EEG measured on human forehead by both ESS (red) and Ag/AgCl electrodes (black). Two frequency spectra of the EEG are well overlapped. 10 Hz alpha rhythm measured by ESS is clearly visible when eyes were closed. d) Skin temperature change measured by epidermal RTD (red) and thermocouple (black) found good correlation. e) Real time skin hydration before and after Espresso intake measured by both commercial coaxial corneometer (black) and ESS (red). f) Voltage outputs from the electrically conductive rubber (ECR) Wheatstone bridge during normal and deep breath.

ear (on the mastoid), as shown in Figure 3c, left panel. Signals were high and low passed filtered at 0.1 and 40 Hz, respectively. Frequency spectra were calculated using standard fast Fourier transformations (FFTs). The remarkable agreement between conventional and ESS measured EEG is evident in Supporting Information Figure S11. Their FFT spectra almost fully overlap in the upper right panel of Figure 3c, which confirms that conventional and ESS electrodes are almost indistinguishable in measuring EEG signals, but the ESS offers additional merits including conformability, softness, and customizable electrode patterns. The lower right panel of Figure 3c compares the FFT of the ESS measured EEG while the subject's eyes were staying open (black) or closed (red). One can note the expected increase in relative alpha power whiles the subject's eyes were closed (centered around 10 Hz).

In addition to EP, skin temperature, skin hydration, and skin deformation are also useful indicators of human physiology. For example, skin temperature is associated with cardiovascular health, cognitive state, and tumor malignancy.[31–33] Skin hydration is widely used in dermatology and cosmetology for the detection of diseases (e.g., eczema, atopic dermatitis, etc.),[34,35] the assessment of mental stress or hormone levels,[36,37] and the evaluation of medical therapies or cosmetic treatments.[38,30] Quantifying skin deformation is useful for the detection of gesture,[39] respiration, as well as motion disorders.[16] Ultrathin, stretchable RTD can be built as a narrow but long ribbon of Au FS as labeled in Figure 2a, which has a high initial resistance R_0 and a predictable change in resistance as the temperature changes. RTD calibration is provided in Supporting Information Figure S12a,b. Strain effect on RTD reading is also investigated. Supporting Information Figure S12c shows that when the RTD is subjected to a tensile strain of 25% (i.e., the elastic limit of skin), the resistance change is within 0.15%, which corresponds to less than 1 °C temperature change. This finding suggests that temperature measurement should be performed under minimal skin deformation. To perform skin temperature measurement, the epidermal RTD was attached on human forearm, along with a commercial thermocouple (TMD-56, Amprobe) as pictured in Figure 3d, left panel. Skin temperature measured by the epidermal RTD (red) and the thermocouple (black) are plotted in Figure 3d, right panel. Skin temperature was initially stabilized at around 30 °C. At t = 2′13″, an ice bag was brought in contact with the RTD and skin for 1 min and then removed. The corresponding temperature drop and recovery are clearly visible in the graph of Figure 3d. The strong correlation between RTD and thermocouple outputs has validated the use of RTD as a soft and stretchable skin temperature detector.

Skin hydration level is reflected by the impedance of skin,[11] which is conveniently measured by impedance sensors in the coaxial dot-ring design as labeled in Figure 2a. Laminating the epidermal hydration sensor (H. sensor) on human skin, an inductance, capacitance, and resistance (LCR) meter (Digital Multimeter, Rigol) was used to measure the impedance at different frequencies as well as different skin hydration levels. A commercial corneometer (MoistureMeterSC Compact, Delfin Inc.) was used to quantify the skin hydration level. Hydration sensor calibration is provided in Supporting Information Figure S13a,b. Figure 3e illustrates a continuous hydration measurement with both epidermal H. sensor and the corneometer before and after the subject drank a can of cold Espresso. The caffeine in Espresso is expected to lead to perspiration as it stimulates human central nervous system, which activates the sweat glands. The results are shown in Figure 3e, right panel, which clearly indicates gradual increase of hydration after drinking Espresso based on the measurements of both the epidermal H. sensor and the corneometer. The initial increase in hydration before drinking Espresso is believed to be caused by the ESS lamination which is discussed in detail in Supporting Information Figure S14. It is also interesting to note that skin hydration peaked 7 min after drinking the Espresso and started to decay after that, likely due to the thermoregulation of the body. An artifact of contact pressure in measuring skin hydration with ESS was noticed and can be prevented as discussed in Supporting Information Figure S15.

Epidermal respiratory rate sensor was build using electrically conductive rubber (ECR), which is similar to our previous soft strain gauge work,[40] but is made by the more cost and time effective "cut-and-paste" method. Unlike conventional microfabrication techniques that are limited to inorganic materials, the "cut-and-paste" process developed here can be applied to a much broader category of materials, including elastomeric sheets. As a demonstration, we fabricated stretchable strain gauges employing ECR (Elastosil LR 3162, Wacker Silicones) as the strain-sensitive resistor, and Au-on-PET serpentine ribbons as the stretchable interconnects (see Supporting Information Figure S16 for details). Sensor validation was performed by applying Tegaderm-supported ECR-based strain gauges on the chest of a human subject (Figure 3f, left picture) and various respirational patterns were measured. Figure 3f, right graph, illustrates the deformation of human chest during normal breath and deep breath using the Wheatstone bridge. Larger amplitude and lower frequency are observed for deep breath.

Compared with silicon nanomembrane[39,41] and ECR[40] based skin-integrated stretchable strain gauges, epidermal strain sensors based on planar stretchable capacitor can operate wirelessly.[13] Instead of using stretchable capacitor, here we explore planar stretchable inductors to build wireless epidermal strain sensors. The double-stranded serpentine design of the planar inductor coil as depicted in Figure 2a has taken into account overall size, stretchability, overall inductance, and strain sensitivity (see Supporting Information). **Figure 4** illustrates the wireless measurement on the sensor coil. A circular reader coil is connected to an Impedance Analyzer (HP 4194A) via a standard BNC-RCA adaptor. The reader coil is inductively coupled to the sensor coil in a transformer like configuration (Figure 4a). The experimental setup is given in Figure 4b and there was no cable connection between the reader and the sensor coil. By measuring the impedance response of the coupled circuit as a function of frequency, the resonance frequency can be determined as the dip in the phase–frequency curve (see details in Supporting Information).

We performed uniaxial stretch tests on Tegaderm supported stretchable coils (Figure 4c) and recorded strain-induced shift of resonance frequency of the coupled circuit, as shown in Figure 4d. Measured resonance frequency as a function of applied strain is plotted in red in Figure 4e, which shows a monotonic decay as the sensor coil is uniaxially elongated. The

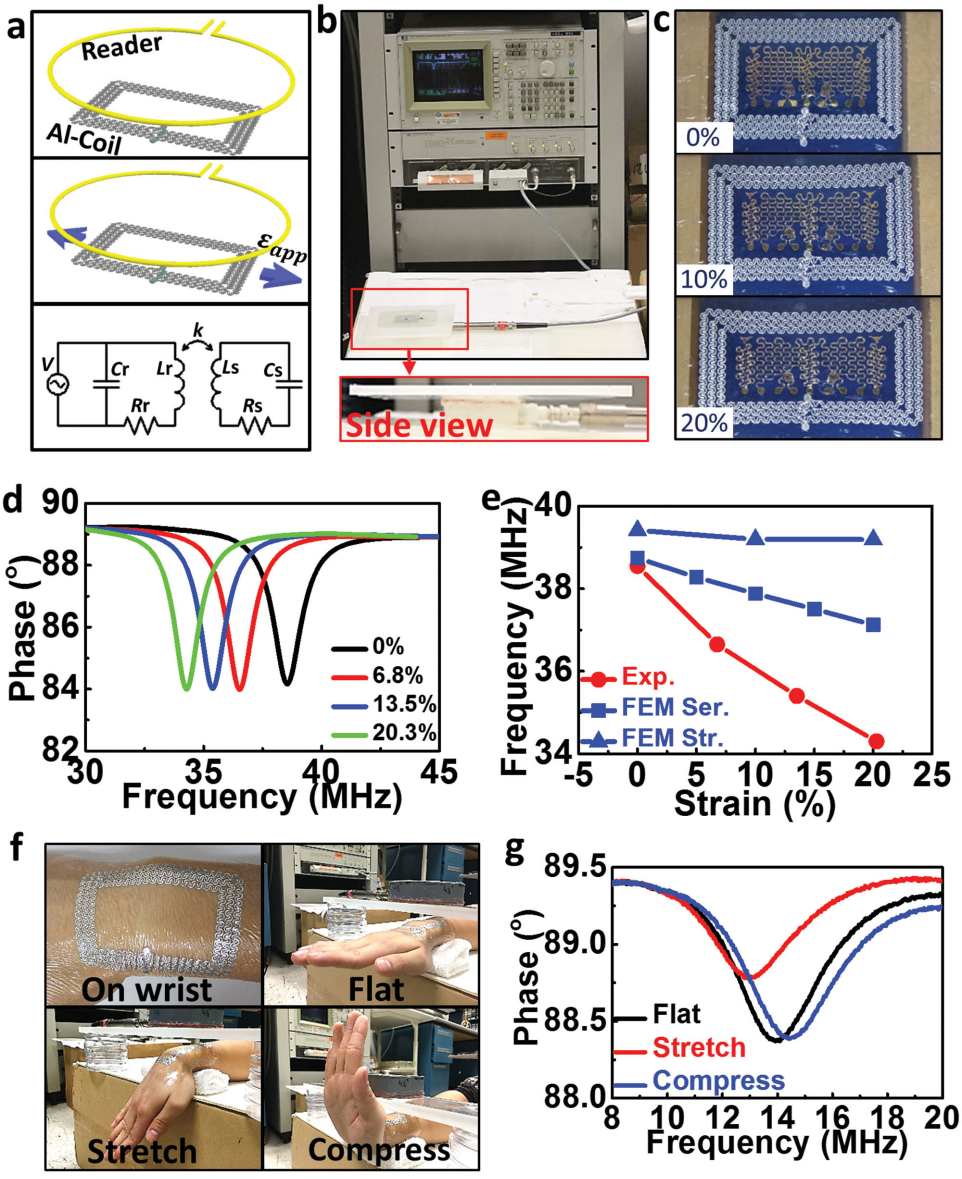

Figure 4. Wireless epidermal strain sensor based on stretchable Al coil. a) Schematics of the wirelessly coupled reader and sensor coils. b) Experimental setup for the measurement of the resonance frequency of the coupled system. The sensor coil was place on top of the reader coil and separated by a 6 mm thick acrylic slab plus 4 mm air gap. The reader was connected to an Impedance Analyzer (HP 4194A). c) Images of the sensor coil stretched horizontally by 0%, 10%, and 20%, respectively. d) Phase response of the coupled system as a function of sweeping frequency at different applied strains. e) Both experimental (red) and FEM (blue) results showing decreased resonance frequency with increased tensile strain. f) Sensor coil attached on human wrist (top left) under different hand gestures: "flat" (top right), "stretch" (bottom left), and "compress" (bottom right). g) Resonance frequency decreases when the sensor coil is stretched by the wrist, and increases when compressed by the wrist.

resonance frequency shifted from 38.6 MHz in the undeformed shape down to 34.3 MHz at the strain of 20%, which is more sensitive to deformation compared to a previously reported stretchable epidermal antenna.[17]

FEM analysis on stretchable coils has been carried out through a combination of ABAQUS standard and ANSYS Maxwell package (see Supporting Information Figure S18 for details) and the results are plotted in blue in Figure 4e, with squares representing serpentine coils (Supporting Information Figure S19a,b) and triangles representing straight coils (Supporting Information Figure S19c,d). Comparing the two results, straight coil appears less sensitive to applied strain, which is undesirable for strain sensing application but could be advantageous for antenna application when stable resonance frequency is needed. Analytical modeling of single and multiturn straight coils is given in Supporting Information Figure S20. All results (experimental, numerical, and analytical) suggest a decay of resonance frequency with increasing uniaxial tensile strain, but the discrepancy between experimental and FEM results requires future studies.

The effect of reader-sensor distance has also been investigated (Supporting Information Figure S21a,b). It is evident

that the resonance frequency does not depend on the distance whereas the phase dip does. Specifically, the smaller the gap, the larger the phase dip, thus the higher coupling factor (*k* factor as labeled in Figure 4a bottom frame). One way to improve the coupling factor and hence enlarge the sensing distance is to increase the overall size of either the reader or the sensor coil, with a tradeoff of course in the wearability of the sensor and the portability of the reader.

Skin deformation measurement was performed by attaching the sensor coil on the dorsal wrist and bringing the reader coil within 45 mm distance from the sensor coil. Three layers of tattoo paper (Silhouette) were applied between the sensor coil and the skin to compensate for capacitive loading induced by the skin. Three wrist gestures "flat," "stretch," and "compress" were measured (Figure 4f). Phase measurement for the three gestures is plotted in Figure 4g, which reveals several interesting findings. First, the resonance frequency drops from 38.6 to 13.92 MHz before and after the sensor coil was applied on the skin, which is due to the substantial capacitive loading induced by the skin.[42] The second observation is that "stretch" reduces the resonance frequency (from 13.92 to 12.99 MHz) whereas "compress" slightly increases resonance frequency (from 13.92 to 14.41 MHz), as expected. Repeatability test was conducted by forming the wrist gestures in the sequence "flat," "stretch," and "compress" twice and the result (Supporting Information Figure S21c,d) shows that the wireless strain gauge coil can offer very repeatable measurements of joint bending.

The planar stretchable coil also has the potential to work as an NFC antenna for transferring signals measured by the ESS wirelessly to a remote receiver.[17] In order to transfer data properly, the resonance frequency should remain as steady as possible during the transferring process. We therefore tested the coil response when it is placed on human chest and the subject was under deep inhalation and exhalation. Supporting Information Figure S21e,f indicates that the resonance frequency only changed from 13.06 to 12.80 MHz, for either deep inhalation or exhalation. The insensitivity of resonance frequency to chest deformation associated inhalation and exhalation makes it possible to be used as a stable epidermal antenna for chest ESS.

In conclusion, we have demonstrated a versatile, cost- and time-effective method to manufacture multimaterial, multiparametric ESS that can be intimately but noninvasively and unobstructively applied on human skin to measure ECG, EMG, EEG, skin temperature, skin hydration, respiratory rate, and joint bending. The "cut-and-paste" method enables completely dry, benchtop, freeform, and portable manufacture of ESS within minutes, without using any vacuum facilities or chemicals. The "cut-and-paste" method has proved effective in patterning metal-on-polymer laminates and elastomeric sheets, but it is not applicable to ceramic-coated polymer as indentation of the cutting blade would easily fracture intrinsically brittle ceramic film. However, we have demonstrated a variation of the "cut-and-paste" method to manufacture highly stretchable transparent interconnects based on brittle indium tin oxide film.[24] In addition to ESS, the "cut-and-paste" manufacturing method is expected to be useful for the manufacture of other stretchable devices including stretchable circuit boards which house rigid IC chips[43] and deployable structure health monitoring sensor networks.[44]

Experimental Section

Fabrication of ECR-Based Stretchable Strain Gauges: The ECR-based stretchable strain gauge was made by a two-step "cut-and-paste" process. The ECR is a clayish, two-component compound which requires thermal curing. The A and B components were first fully mixed by a drill mixer in a 1:1 ratio in weight and then squeezed by two parallel acrylic slabs pressured by binder clips. The squeezed ECR compound along with the acrylic slab and binder clips was then put into an oven in 70 °C for 4 h. After curing, an ECR film was obtained and the thickness of the ECR film turned out to be 120–140 μm. The ECR film was then cut and pasted onto Tegaderm to form the resistor and Wheatstone bridge. The Au-on-PET foil was then cut and pasted onto the same Tegaderm guided by alignment markers to form the serpentine interconnects of the strain gauges.

Measurement and Processing of EEG: For EP measurements, conventional and ESS channels were amplified using the AvatarEEG system in 24 bit DC mode at an initial sampling rate of 500 Hz. EEG signals were recorded with respect to the mastoid reference channel across a 297 s recording epoch. Offline, the data were then bandpass-filtered between 0.1 and 40 Hz and then visually inspected for artifacts and blinks. Contaminated sections were removed from the analysis. Artifact-free EEG data were then divided into two conditions: a 52 s epoch of resting eyes opened and a 52 s epoch of resting eyes closed. Spectral power measures were computed for each condition via FFT with a Hamming window.

Experiments on Human Subjects: Informed signed consent was obtained from all human test participants.

Supporting Information

Supporting Information is available from the Wiley Online Library or from the author.

Acknowledgements

S.Y., Y.-C.C., L.N., P.P., B.S., R.Y., N.L., D.N., and D.S. conducted device design, fabrication, calibration, and testing. S.Y. led the FEM analysis with the assistance of J.S. D.S. Y.C., P.W., S.Y., Y.-C.C., L.N., and R.Y. served as human subjects. L.N. and D.S. performed EP analysis. N.L., D.N., and D.S. supervised and coordinated the project. N.L., S.Y., Y.-C.C., L.N., P.P., D.N., and D.S. wrote the paper. This work is based upon work supported in part by the National Science Foundation under Grant Nos. CMMI-1301335 and CMMI-1351875 (CAREER). N.L. acknowledges the 3M Non-Tenured Faculty Award. Any opinions, findings, and conclusions or recommendations expressed in this material are those of the authors and do not necessarily reflect the views of the National Science Foundation nor 3M.
This article was modified on November 4, 2015. The author names B. Su and D. Sanchez were corrected.

Received: May 19, 2015
Revised: August 5, 2015
Published online: September 23, 2015

[1] N. Bowden, S. Brittain, A. G. Evans, J. W. Hutchinson, G. M. Whitesides, *Nature* **1998**, *393*, 146.
[2] J. R. Ives, S. M. Mirsattari, D. Jones, *Clin. Neurophysiol.* **2007**, *118*, 1633.
[3] G. Schwartz, B. C. K. Tee, J. G. Mei, A. L. Appleton, D. H. Kim, H. L. Wang, Z. N. Bao, *Nat. Commun.* **2013**, *4*, 1859.
[4] S. Gong, W. Schwalb, Y. W. Wang, Y. Chen, Y. Tang, J. Si, B. Shirinzadeh, W. L. Cheng, *Nat. Commun.* **2014**, *5*, 3132.
[5] S. Gong, D. T. H. Lai, B. Su, K. J. Si, Z. Ma, L. W. Yap, P. Guo, W. Cheng, *Adv. Electron. Mater.* **2015**, *1*, DOI: 10.1002/aelm.201400063.

[6] D. H. Kim, R. Ghaffari, N. S. Lu, J. A. Rogers, *Annu. Rev. Biomed. Eng.* **2012**, *14*, 113.
[7] D. H. Kim, N. L. Lu, R. Ghaffari, J. A. Rogers, *NPG Asia Mater.* **2012**, *4*, e15.
[8] D. H. Kim, N. S. Lu, R. Ma, Y. S. Kim, R. H. Kim, S. D. Wang, J. Wu, S. M. Won, H. Tao, A. Islam, K. J. Yu, T. I. Kim, R. Chowdhury, M. Ying, L. Z. Xu, M. Li, H. J. Chung, H. Keum, M. McCormick, P. Liu, Y. W. Zhang, F. G. Omenetto, Y. G. Huang, T. Coleman, J. A. Rogers, *Science* **2011**, *333*, 838.
[9] X. Feng, B. D. Yang, Y. M. Liu, Y. Wang, C. Dagdeviren, Z. J. Liu, A. Carlson, J. Y. Li, Y. G. Huang, J. A. Rogers, *ACS Nano* **2011**, *5*, 3326.
[10] Y. Hattori, L. Falgout, W. Lee, S. Y. Jung, E. Poon, J. W. Lee, I. Na, A. Geisler, D. Sadhwani, Y. H. Zhang, Y. W. Su, X. Q. Wang, Z. J. Liu, J. Xia, H. Y. Cheng, R. C. Webb, A. P. Bonifas, P. Won, J. W. Jeong, K. I. Jang, Y. M. Song, B. Nardone, M. Nodzenski, J. A. Fan, Y. G. Huang, D. P. West, A. S. Paller, M. Alam, W. H. Yeo, J. A. Rogers, *Adv. Healthcare Mater.* **2014**, *3*, 1597.
[11] X. Huang, W. H. Yeo, Y. H. Liu, J. A. Rogers, *Biointerphases* **2012**, *7*, 1.
[12] X. Huang, H. Cheng, K. Chen, Y. Zhang, Y. Zhang, Y. Liu, C. Zhu, S.-c. Ouyang, G.-W. Kong, C. Yu, Y. Huang, J. A. Rogers, *IEEE Trans. Biomed. Eng.* **2013**, *60*, 2848.
[13] N. Lu, D. H. Kim, *Soft Robotics* **2013**, *1*, 53.
[14] A. J. Bandodkar, D. Molinnus, O. Mirza, T. Guinovart, J. R. Windmiller, G. Valdes-Ramirez, F. J. Andrade, M. J. Schoning, J. Wang, *Biosens. Bioelectron.* **2014**, *54*, 603.
[15] X. Huang, Y. H. Liu, K. L. Chen, W. J. Shin, C. J. Lu, G. W. Kong, D. Patnaik, S. H. Lee, J. F. Cortes, J. A. Rogers, *Small* **2014**, *10*, 3083.
[16] D. Son, J. Lee, S. Qiao, R. Ghaffari, J. Kim, J. E. Lee, C. Song, S. J. Kim, D. J. Lee, S. W. Jun, S. Yang, M. Park, J. Shin, K. Do, M. Lee, K. Kang, C. S. Hwang, N. S. Lu, T. Hyeon, D. H. Kim, *Nat. Nanotechnol.* **2014**, *9*, 397.
[17] J. Kim, A. Banks, H. Cheng, Z. Xie, S. Xu, K.-I. Jang, J. W. Lee, Z. Liu, P. Gutruf, X. Huang, P. Wei, F. Liu, K. Li, M. Dalal, R. Ghaffari, X. Feng, Y. Huang, S. Gupta, U. Paik, J. A. Rogers, *Small* **2015**, *11*, 906.
[18] M. A. Pacheco, C. L. Marshall, *Energy Fuel* **1997**, *11*, 2.
[19] N. S. Lu, X. Wang, Z. Suo, J. Vlassak, *Appl. Phys. Lett.* **2007**, *91*, 221909.
[20] H. Seitz, S. Marlovits, I. Schwendenwein, E. Muller, V. Vecsei, *Biomaterials* **1998**, *19*, 189.
[21] J. W. Jeong, W. H. Yeo, A. Akhtar, J. J. S. Norton, Y. J. Kwack, S. Li, S. Y. Jung, Y. W . Su, W. Lee, J. Xia, H. Y. Cheng, Y. G. Huang, W. S. Choi, T. Bretl, J. A. Rogers, *Adv. Mater.* **2013**, *25*, 6839.
[22] T. Widlund, S. Yang, Y.-Y. Hsu, N. Lu, *Int. J. Solids Struct.* **2014**, *51*, 4026.
[23] F. M. Hendriks, *Universiteitsdrukkerij TU Eindhoven*, Eindhoven, The Netherlands **2005**.
[24] S. Yang, E. Ng, N. Lu, *Extreme Mech. Lett.* **2015**, *2*, 37.
[25] V. Arumugam, M. D. Naresh, R. Sanjeevi, *J. Biosci.* **1994**, *19*, 307.
[26] N. V. Thakor, Y. S. Zhu, *IEEE Trans. Biomed. Eng.* **1991**, *38*, 785.
[27] W. Klimesch, *Brain Res. Rev.* **1999**, *29*, 169.
[28] F. Rosenow, K. M. Klein, H. M. Hamer, *Expert Rev. Neurotherapeutics* **2015**, *15*, 425.
[29] K. G. Jordan, *J. Clin. Neurophysiol.* **2004**, *21*, 341.
[30] M. Boguniewicz, N. Nicol, K. Kelsay, D. Y. M. Leung, *Semin. Cutan. Med. Surg.* **2008**, *27*, 115.
[31] C. R. Wyss, G. l. Brengelm, J. M. Johnson, L. B. Rowell, M. Niederbe, *J. Appl. Physiol.* **1974**, *36*, 726.
[32] T. M. Makinen, L. A. Palinkas, D. L. Reeves, T. Paakkonen, H. Rintamaki, J. Leppaluoto, J. Hassi, *Physiol. Behav.* **2006**, *87*, 166.
[33] E. Y. K. Ng, *Int. J. Therm. Sci.* **2009**, *48*, 849.
[34] C. Blichmann, J. Serup, *Contact Dermatitis* **1987**, *16*, 155.
[35] K. L. E. Hon, K. Y. Wong, T. F. Leung, C. M. Chow, P. C. Ng, *Am. J. Clin. Dermatol.* **2008**, *9*, 45.
[36] P. G. Sator, J. B. Schmidt, T. Rabe, C. C. Zouboulis, *Exp. Dermatol.* **2004**, *13*, 36.
[37] B. W. Tran, A. D. P. Papoiu, C. V. Russoniello, H. Wang, T. S. Patel, Y. H. Chan, G. Yosipovitch, *Acta Derm. Venereol.* **2010**, *90*, 354.
[38] S. M. Kleiner, *J. Am. Diet Assoc.* **1999**, *99*, 200.
[39] M. Ying, A. P. Bonifas, N. S. Lu, Y. W. Su, R. Li, H. Y. Cheng, A. Ameen, Y. G. Huang, J. A. Rogers, *Nanotechnology* **2012**, *23*, 344004.
[40] R. Kandasamy, X. Q. Wang, A. S. Mujumdar, *Appl. Therm. Eng.* **2008**, *28*, 1047.
[41] D. H. Kim, R. Ghaffari, N. S. Lu, S. D. Wang, S. P. Lee, H. Keum, R. D'Angelo, L. Klinker, Y. W. Su, C. F. Lu, Y. S. Kim, A. Ameen, Y. H. Li, Y. H. Zhang, B. de Graff, Y. Y. Hsu, Z. J. Liu, J. Ruskin, L. Z. Xu, C. Lu, F. G. Omenetto, Y. G. Huang, M. Mansour, M. J. Slepian, J. A. Rogers, *Proc. Natl. Acad. Sci. USA* **2012**, *109*, 19910.
[42] E. Kinnen, *Med. Electron. Biological Eng.* **1965**, *3*, 67.
[43] S. Xu, Y. H. Zhang, L. Jia, K. E. Mathewson, K. I. Jang, J. Kim, H. R. Fu, X. Huang, P. Chava, R. H. Wang, S. Bhole, L. Z. Wang, Y. J. Na, Y. Guan, M. Flavin, Z. S. Han, Y. G. Huang, J. A. Rogers, *Science* **2014**, *344*, 70.
[44] G. Lanzara, N. Salowitz, Z. Q. Guo, F. K. Chang, *Adv. Mater.* **2010**, *22*, 4643.